HHS Public Access

Author manuscript

J Mol Med (Berl). Author manuscript; available in PMC 2016 September 01.

Published in final edited form as:

J Mol Med (Berl). 2015 September ; 93(9): 991–1001. doi:10.1007/s00109-015-1279-x.

Nanoparticles coated with the tumor-penetrating peptide iRGD reduce experimental breast cancer metastasis in the brain

Amanda M. Hamilton[1], **Sallouha Aidoudi-Ahmed**[2], **Shweta Sharma**[2], **Venkata R. Kotamraju**[2], **Paula J. Foster**[1], **Kazuki N. Sugahara**[2], **Erkki Ruoslahti**[2,3], and **Brian K. Rutt**[4]

Amanda M. Hamilton: hamilton@robarts.ca

1

2

3

4

Abstract

Metastasis is the main killer in cancer; consequently, there is great interest in novel approaches to prevent and treat metastatic disease. Brain metastases are particularly deadly, as the protection of the blood-brain barrier obstructs the passage of common anticancer drugs. This study used magnetic resonance imaging (MRI) to investigate the therapeutic effects of nanoparticles coated with a tumor-penetrating peptide (iRGD) against a preclinical model of breast cancer brain metastasis. Single doses of iRGD nanoparticle were administered intravenously, and the effect on tumor growth was observed over time. iRGD nanoparticles, when applied in the early stages of metastasis development, strongly inhibited tumor progression. Overall, this study demonstrated for the first time that a single dose of iRGD nanoparticle can have a significant effect on metastatic tumor progression and nonproliferative cancer cell retention when applied early in course of tumor development. These data suggest that iRGD nanoparticles may be useful in preventatively reducing metastasis after a cancer diagnosis has been established.

Keywords

Brain metastasis; Tumor growth inhibition; Magnetic resonance imaging; iRGD; Nanoparticle; Cell tracking

Background

As systemic therapies that control extracranial cancers improve, patients are surviving longer and the incidence of metastasis to the brain is on the rise [1]. The management of patients with brain metastases from breast cancer continues to be a significant clinical challenge, as brain metastases remain incurable. Of particular concern is the treatment of

Conflict of interest K.N.S., V.R.K., and E.R. have ownership interest (including patents) in CendR Therapeutics Inc., and E.R. is a founder, chairman of the board, and consultant/advisory board member of the company. ER is also a consultant/advisory board member and shareholder of EnduRx Pharmaceuticals Inc. and has ownership interest (including patents) in the same. No other authors have conflicts of interest.

brain metastases in patients with triple-negative breast cancer. Retrospective analysis of triple-negative patient data has revealed a high incidence of brain metastasis with a short latency and shortest median overall survival after intracranial tumor development than in other subtypes of breast cancer [2, 3]. Consequently, there is an increasing interest in novel ways of detecting, preventing, and eventually treating triple-negative breast cancer brain metastases.

One strategy is to development new diagnostic methods and therapies based on novel molecular targets. The α_v integrins, particularly $\alpha_v\beta_3$ and $\alpha_v\beta_5$, are useful molecular targets because they are overexpressed on many tumor-associated cell types, including angiogenic endothelial cells, tumor fibroblasts, tumor macrophages, and many cancer cells themselves [4–6]. The arginine-glycine-aspartic acid (RGD) sequence is an essential binding motif for α_v integrins [6]. Recently, an RGD-containing peptide with novel tumor-penetrating properties has been discovered [7]. This peptide, iRGD, uses the RGD motif to home to tumors by binding to α_v integrins. Proteolytic processing of iRGD then unmasks a second sequence motif, the cryptic CendR motif (R/KXXR/ K), which binds to neuropilin-1 and activates an endocytic bulk transport pathway through tumor tissue. Once activated, this pathway can take iRGD-bound and unbound payloads deep into tumor tissue in mouse models and in human tumor explants [7–12]. In addition to these properties, iRGD has recently been found to have anti-metastatic properties; prolonged treatment of tumor mice strongly inhibited the development of metastases in two tumor models [13].

We have investigated the activity of iRGD on the formation of brain metastases employing high-resolution magnetic resonance imaging (MRI) and two mouse models of triple-negative metastatic breast cancer. Our focus was on a nanoworm (NW, nanoparticles so-called because of their elongated shape)-bound formulation of iRGD. Administered cancer cells were first labeled in vitro with iron oxide (IO). The IO label creates a magnetic field disturbance that could be detected in magnetic resonance images as signal voids [14, 15]. This technology has become a valuable tool for studying the in vivo trafficking of transplanted cells and allows the visualization of the initial delivery and distribution of cells. IO labeling also allows the differentiation of highly proliferative cells from dormant entities. As cells divide, the IO label is diluted beyond the detection limit and hyperintense micrometastases form in their stead. Persistent signal voids in MR images represent nonproliferative cancer cells that remain dormant in the brain and retained their IO label over time. A key aspect to this study was to use this technology to simultaneously track the response to treatment of both the nonproliferating iron-labeled cancer cell population and the macroscopic tumor burden in two independent breast cancer brain metastasis models.

Methods

Cell culture and micron-sized iron oxide labeling

MDA-MB-231BR eGFP-positive (231BR) and 4T1-BR5 cells were each maintained in Dulbecco's modified Eagle's medium (DMEM) containing 10 % FBS at 37 °C and 5 % CO_2. For in vitro IO labeling, 2×10^6 adherent cells were incubated with 25 μg Fe/mL MPIO beads (0.9 μm, labeled with Flash Red; Bangs Laboratory, Fisher, IN, USA) for 24 h. Cell

labeling had no effect on cell viability, and labeling efficiency was assessed by Perl's Prussian blue (PPB) staining.

Animal model

To deliver IO-labeled cells to the entire mouse brain, cells were injected into the left ventricle of anesthetized female mice (6–8 weeks old; Charles River Laboratories, Wilmington, MA, USA). Nu/nu Foxn1 mice were used for the 231BR model, and BalbC mice were used for the 4T1-BR5 model. The animals were cared for in accordance with the standards of the Canadian Council on Animal Care under an approved protocol from the University of Western Ontario's Council on Animal Care. Cells were delivered by intracardiac (left ventricle) injection into anesthetized mice. Mice received either 1.5×10^5 IO-labeled 231BR cells or 2×10^4 IO-labeled 4T1-BR5 cells over a 20-s time period. The mice were monitored until awake and fully active. As described later, mice were imaged within 24 h post-injection to confirm successful cell delivery. Mice were monitored by weight and visual inspection for any signs of stress or severe illness until endpoint. For the 231BR model, monitoring occurred biweekly from days 0 to 24 and daily thereafter until endpoint. For the 4T1-BR5 model, mice were monitored every 2 days from days 0 to 10 and daily thereafter until endpoint. Animals were sacrificed when poor body condition was evident (prominence of pelvis and vertebrae segmentation) or >20 % weight loss or severe health complication (full hind limb paralysis, severe head tilt, or spontaneous seizure) was observed.

Peptide synthesis and nanoworms

The iRGD (tumor penetrating) and CRGDC (nonpenetrating) peptides were synthesized with an extracysteine residue to provide a free sulfhydryl group for coupling purposes, purified to >90 % purity, and coupled to IO nanoworms (NWs) as previously described [16].

Administration of treatment

Only mice that presented with MR signal voids post-cell injection were included in the studies.

231BR model: for treatment day (td) 6 and td 12 experiments, 231BR cell-injected mice were injected intravenously with either 100 μL saline (td 6/12 *n*=5), 5 mg/kg of iRGD-NWs (td 6 *n*=6, td 12 *n*=5), or 5 mg/kg CRGDC-NWs (td 6 *n*=6, td 12 *n*=5) in 100 μL saline on their respective td. For the free peptide and bound NW comparison experiment, cell-injected mice were injected intravenously on day 7 with 100 μL saline (*n*=10), 100 μg/mouse of soluble iRGD peptide (*n*=9), or 5 mg/kg of iRGD-NWs (*n*=9) in the same volume of saline. All injections were successfully administered.

4T1-BR5 model: 4T1-BR5 cell-injected mice were injected intravenously with 100 μL saline (*n* =4), 5 mg/kg iRGD-NWs (*n*=4), or 5 mg/kg CRGDC-NWs (*n*=4) in 100 μL saline on day 2 post-cell injection. All injections were successfully administered.

Magnetic resonance imaging

All MRI examinations were performed on a 3T GE Discovery MR750 whole-body clinical MR scanner using a custom-built high-performance gradient coil (maximum gradient strength= 500 mT/m and peak slew rate=3000 T/m/s) and a custom solenoid radiofrequency mouse head coil (1.5-cm inner diameter). For imaging, mice were anesthetized using 2 % isoflurane in 100 % O_2. All mice were imaged within 24 h post-cell injection to determine injection efficiency using a 3-D bSSFP sequence with the following parameters: resolution, 100×100×200 μm^3; repetition time/echo time (TR/TE)=8/ 4 ms; flip angle=35°; bandwidth= ±42 kHz; four phase cycles; and scan time, 14 min [17]. Mice were imaged to assess tumor growth over time under the different treatment conditions.

231BR model: mice grouped into td 6 and 12 experiments were imaged on days 23 and 30 post-cell injection. Mice grouped into the free peptide and bound NW experiment were imaged on day 25 post-cell injection.

4T1-BR5 model: mice were imaged on days 10 and 15 post-cell injection because these tumors grow faster than the 231BR tumors.

All tumor assessment imaging was done using a 3-D bSSFP sequence with the following parameters: resolution, 100×100×200 μm^3; TR/TE=10/5 ms; flip angle=35°; band-width= ±12.5 kHz; eight phase cycles; number of excitations, two; and scan time, 36 min. No animals were lost during the imaging procedures.

Magnetic resonance image analysis

All images were viewed and analyzed using OsiriX image software (open source). To estimate cell delivery, MR images from within 24 h post-cell delivery were assessed. Approximately 120 bSSFP images spanned each individual mouse brain, manually counting signal voids in ten random images and multiplying by a factor of 12 estimated cell delivery. For the entire study, a total of 58 nu/nu mice received intracardiac injections of 231BR cells and 32 BalbC mice received intracardiac injections of 4T1-BR5 cells. MRI analysis revealed four nu/nu mice, and nine BalbC mice had insufficient cell delivery and were therefore excluded from further study. Eleven further BalbC mice had to be excluded before the conclusion of the study for severe health complications. The remaining mice were assigned to treatment groups with approximately the same average cell delivery. Cell delivery estimates were also used in void retention calculations at later MR image time points.

231BR model: MR images from days 23, 25, and 30 were assessed for number of tumors, total tumor volume, and signal void retention.

4T1-BR5 model: MR images from days 10 and 15 were assessed for number of tumors, total tumor volume, and signal void retention.

A blinded single observer performed all analysis. Tumor numbers were counted, and volumes were calculated using manual hand tracing. A volume calculation algorithm in OsiriX determined the volume of each individual metastasis. Signal void retention is presented as percent retained voids in relation to the number of cells estimated to have initially arrested post-cell injection. All MR data was summarized for each individual mouse, and summary data was compared across treatment groups.

Tissue collection

Animals in the iRGD-NW vs CRGDC-NW comparison mice were sacrificed at their respective imaging endpoints (days 15 or 30). Animals in the NW and soluble peptide comparison experiment were assessed for altered survival. The health status of these animals was monitored on a daily basis until health failure was observed as an overnight 20 % weight loss. All mice were sacrificed by a pentobarbital (Euthanyl) overdose. After sacrifice, mice were perfused with a 0.9 % saline solution, followed by 10 % formalin.

Tissue processing and histological analysis

Fixed mouse brains were paraffin-embedded and sectioned at 5 μm. Select sections were deparaffinized and stained with hematoxylin and eosin (H&E) to examine tumor morphology and MR imaging validation. Coregistration of images was based on the alignment of anatomical landmarks. For the 231BR model, a select number of neighboring tissue sections were used to perform immunohistochemistry for the proliferation marker Ki67 (1/200 dilution, rabbit monoclonal antibody Clone SP6, Cat# RM-9106-S, Thermo Fisher Scientific, USA). All microscopy was performed on a Zeiss AXIO Imager (Carl Zeiss Canada Ltd, Canada).

Statistical analysis

All statistical analysis was performed using GraphPad Prism software (Version 6.0, GraphPad Software, Inc., USA). Data with multiple imaging time points was assessed with repeated measures two-way analysis of variance (ANOVA) examining the effects of treatment and time. Data with a single time point was assessed with one-way ANOVA evaluating treatment effect. All statistical tests were also evaluated by Tukey post hoc test.

Results

Detection of labeled cells and metastasis growth

PPB staining showed the presence of iron particles within 87–99 and 92–95 % of IO-labeled 231BR and 4T1-BR5 cells, respectively (Fig. 1a, b). The iron labeling did not have any significant effect on cell viability, as 95–98 % of 231BR cells and 90–94 % of 4T1-B5 cells were found viable by Trypan blue exclusion assay. A representative image of successful cell delivery into the brain is shown in Fig. 1c, d. The bSSFP image sequence used was sensitive to field inhomogeneity including that caused by the IO. Imaging mice within 24 h of an IO-labeled cell injection using bSSFP permitted the estimation of cell delivery and also enabled the assessment of signal void retention over time. There was no statistically significant difference in cell delivery for each of the examined mouse groups.

At later time points, metastases appeared as high-signal-intensity regions in bSSFP images due to their high fluid content in relation to normal brain parenchyma (Fig. 2b, c, e, f). Total tumor burden increased over time in all mice imaged in this study, and bSSFP imaging permitted the evaluation of individual tumor growth over time (Fig. 2b, c, e, f shows examples of growing tumors as indicated by the black arrows), as well as the identification of new tumors (Fig. 2c, f shows examples of new tumors as indicated by the gray arrows).

The brains of a subset of mice from each experimental model were excised at endpoint and assessed histologically for the presence of tumors (representative images are shown in Fig. 3b, e). High-magnification images of H&E-stained sections (Fig. 3c) showed the typical tumor morphology for 231BR tumor growth in nude mouse brain [17, 18]. Metastases were evident as packed cell clusters surrounded by regions of edema appearing as large white spaces in histological sections. High-magnification images of 4T1-BR5 tumors (Fig. 3f) showed less edema surrounding cancer cell clusters than in the 231BR tumors. The tumors observed in bSSFP images in both cancer models correlated well with the tumors identified in the histology.

Effect of iRGD on metastasis development in the 231BR model

We compared the metastasis development from injected 231BR breast cancer cells in mice administered with a single intravenous dose of iRGD-NWs, vehicle control, or NWs conjugated with a conventional RGD peptide CRGDC (CRGDC-NWs). The CRGDC peptide binds to α_v integrins but lacks the tumor-penetrating properties of iRGD [7]. MRI analysis at 30 days after cell injection using a 3-D bSSFP sequence showed that iRGD-NW administration at td 6 reduced the number of tumors in the brain by about 60 % compared to the vehicle and CRGDC-NW groups ($p<0.0001$; Fig. 4a). The total tumor volume was about fivefold lower in the iRGD-NW group than in the control groups ($p<0.0004$; Fig. 4b). The vehicle and CRGDC-NW groups did not differ from one another in either parameter. Imaging a week earlier gave similar results, although the difference in the number of tumors was not yet statistically significant. Void retention (the persistence of nonproliferating tumor cells in the brain) was significantly reduced in both the iRGD-NWand CRGDC-NW groups (Fig. 4c), indicating that this activity shared by the two RGD peptides was not responsible for the anti-metastatic effect of the iRGD-NWs. All of these effects disappeared when the NW treatment was postponed to day 12 after the tumor cell injection (Fig. 4d–f). This result indicated that the window for metastasis reduction after tumor cell injection was shorter than 12 days in this mouse model.

Immunohistochemistry for the proliferation marker Ki67 was used to assess the proliferative potential of endpoint tumors. An example image of Ki67-positive staining nuclei is shown in Fig. 5a. In mice treated at day 6, there was a significant difference in the percent of nuclei stained between each group with the highest differential observed between saline control (54.0±4.4 %) and iRGD-NW-treated tumors (36.0± 7.3 %) (Fig. 5b, $p=0.0005$). Mice treated at day 12 showed a significantly lower percentage of positively staining nuclei in CRGDC-NW- and iRGD-NW-treated groups compared to control tumors (one-way ANOVA, $p<0.0001$). This reduction in Ki67 expression was not sufficient, however, to impede tumor progression as tumor growth was observed for all groups.

Comparison of the activities of nanoworm-bound iRGD and free peptide

Multivalent presentation of a peptide on a nanoparticle can enhance the activity of the peptide [11, 16, 19]. We therefore tested whether conjugation of the iRGD peptide to NW results in any alteration of treatment efficacy compared to free iRGD peptide. All MRI analysis for this experiment was performed on day 25 post-231BR cell injection. In agreement with the results shown above, iRGD-NW-treated mice exhibited a significantly

lower tumor number and total tumor volume than the vehicle control mice (Fig. 6a, b). In contrast, mice injected with a dose of iRGD peptide exhibited tumor number and volumes that were not statistically different from in the vehicle control. These results suggest that the nanoparticle presentation potentiates the activity of the iRGD peptide.

We also determined the effect of iRGD-NWs on the survival of the mice injected with the metastatic cells. The iRGD-NW-treated mice exhibited prolonged survival with median death at 37 days compared to saline (32 days) or the free iRGD peptide (32 days). Statistically, a Mantel-Cox test did not find significant difference between the survival curves (ns p=0.1085); however, the logrank test for trend was significant (p=0.043) indicating a significant trend for greater survival in the iRGD-NW treatment group.

Effect of iRGD on metastasis development in the 4T1-BR5 model

We next sought to investigate whether the reduction in tumor burden by iRGD-NW treatment observed in the 231BR model could be duplicated using another breast cancer brain metastasis model. We used the murine model of triple-negative breast cancer brain metastasis, 4T1-BR5 cell line, which has been through multiple rounds of brain selection to derive cells with preferential growth in mouse brain [20]. This cancer model is significantly more aggressive than the 231BR model, and thus, both treatment and MRI scan days were adjusted accordingly. We compared the metastasis development from injected 4T1-BR5 breast cancer cells in mice administered with a single intravenous dose of saline, CRGDC-NW or iRGD-NWs, at day 2 post-cell injection. There was no significant difference in cell delivery between the treatment groups (Fig. 7a). Mice in this model suffered from a variety of health deficits including limb paralysis, seizures, and severe head tilt that required the early sacrifice of multiple animals. Final data analysis only included mice that survived to the predetermined endpoint (day 15) and could be MR imaged prior to sacrifice. MRI analysis at day 10 showed statistically fewer tumors and less total tumor volume in mice injected with iRGD-NW at td 2 than saline control animals (Fig. 7b, c, p=0.0002). Imaging results at endpoint showed that iRGD-NW administration reduced the number of tumors in the brain by more than 50 % compared to the saline control group (p= 0.025; Fig. 7b). The total tumor volume was more than threefold lower in the iRGD-NW group than in the two comparison groups (p=0.02; Fig. 7c). The vehicle and CRGDC-NW groups did not differ from one another in either parameter. At day 10, void retention was significantly reduced in both the iRGD-NW and CRGDC-NW groups (Fig. 7d) when compared to saline control. This significant difference was not observed at endpoint (day 15). Overall, the experimental results observed using the 4T1-BR5 model are in agreement with those seen using the 231BR model.

Discussion

In the present study, we used in vivo MRI to study the anti-metastatic properties of iRGD-conjugated NWs in two experimental breast cancer brain metastasis models. We show that iRGD-NWs reduced metastatic tumor growth, that this activity was not shared by NWs conjugated to a conventional RGD peptide (CRGDC), and that the NW-bound iRGD was

more effective than free iRGD peptide. Remarkably, the iRGD-NWs inhibited the development of intracranial metastases after only one systemically administered dose.

We performed the study in two mouse models of triple-negative breast cancer brain metastasis: the nu/nu mouse MDA-MB-231BR model [17, 18, 21, 22] and the BalbC mouse 4T1-BR5 model. In the 231BR model, the blood-brain barrier (BBB) has previously been shown to remain intact in early stages of disease progression [17]; thus, to be effective, any therapeutic applied early in the course of development needed to be able to traverse an intact BBB. We used MRI to study the growth of brain metastases longitudinally with high spatial resolution, good tumor to normal tissue contrast, and single-cell sensitivity. These properties made it possible to detect initial tumor cell arrest in the brain of an intact mouse and then follow the growth of a subset of these cells into metastatic lesions [17]. A key aspect to this study was our ability to simultaneously track nonproliferating iron-labeled cancer cells and tumor progression over time. Individual persisting cancer cells may be able to form late-developing metastases, as has been reported for preclinical breast cancer metastases in the liver [23]. Thus, the evaluation of the effect of a potential therapeutic on both the proliferating and dormant cancer cell populations was a substantial advancement.

A single dose of iRGD-NWs administered 6 days after an intravenous injection of tumor cells successfully reduced 231BR tumor formation in the brain.

The NWs, however, were ineffective when given 12 days after the tumor cell injection, showing that the treatment window in the 231BR model was limited in duration. A similar time dependency has previously been observed in a pre-clinical therapeutic trial performed by Fitzgerald et al. using the 231BR model [24]. In that study, authors used histological analysis to compare the efficacy of multiple doses of the microtubule-stabilizing drug TPI-287 and compared it to paclitaxel treatment applied either early (days 3, 7, and 11) or late (days 18, 22, and 26). Paclitaxel had no observable effect on tumor growth irrespective of treatment timing. TPI-287, however, significantly reduced the number of large brain metastases by a significant 55 % when applied early but did not significantly alter tumor growth when applied late. The results of our study in combination with those of Fitzgerald et al. suggest that delayed treatment in aggressive tumor models is not sufficient to control tumor growth in established micrometastases. Both tumor lines used in our study proliferate rapidly in vivo and were selected to be proficient in brain tumor growth. Patient tumors, which grow much more slowly, may provide a longer window of opportunity to prevent metastatic growth after tumor cell dissemination. Prolonged treatment with soluble iRGD peptide initiated before metastasis development has recently been shown to inhibit spontaneous breast cancer metastasis to various tissues with no or minor effect on the growth of the primary tumor [13]. The present findings, together with this previously published data, suggest a considerable potential of iRGD in metastasis prevention.

Another key observation in our current study was that unlike iRGD-NWs, CRGDC-NWs did not inhibit the growth of brain metastases. Both iRGD and CRGDC bind to α_V integrins, and their affinities are similar. Some RGD peptides have been found to inhibit tumor growth [25–29], but iRGD and CRGDC do not significantly affect the growth of primary tumors [7, 9]. The key difference between iRGD and CRGDC is that, having bound to the integrin,

iRGD is proteolytically processed to expose a neuropilin-1-binding motif, which CRGDC does not possess [7]. Thus, the anti-metastatic activity of iRGD is likely to be mediated by the neuropilin binding. Neuropilin-binding peptides have been shown to inhibit tumor growth [30–34]; however, the activity of these peptides against metastastic growth has not been studied. Moreover, as neuropilin-1 is ubiquitously expressed in tissues, such peptides lack the specificity of iRGD, which is only activated in tumors, not in normal tissues [7].

The iRGD-NW and CRGDC-NW peptides shared one activity: both reduced the retention of signal voids in MR images, which are believed to represent iron-labeled cancer cells lodged in the brain but at least temporarily growth arrested. Since the reduction of these cells had no effect on metastasis development, they are unlikely to contribute to metastatic tumor development within the time frame that we studied. It may be that these cells represent a subpopulation of tumor cells that are incapable of executing the final steps in the metastatic cascade and consequently remain dormant. As the iRGD and CRGDC peptides share integrin-blocking activity, this dormant cell population may rely on integrin-mediated adhesion to remain lodged in the brain vessels. Tumor cell integrin $\alpha_v\beta_3$ has been shown to be required for blood-borne metastasis [35]. The cells that successfully form metastases appear to have passed beyond the stage that requires the integrin.

A single injection of free iRGD peptide showed a trend toward reducing tumor burden from brain metastasis, but the effect did not reach the statistical significance observed in mice treated with iRGD-NWs. The likely reasons for the superior activity of the nanoparticle-bound iRGD include greater avidity for the target cells resulting from the multivalent presentation of the peptide on the nanoparticles (the peptide serves both as a homing device and active agent). Nanoparticles have been popular vehicles for the delivery of anticancer treatments to tumor sites, as these formulations can modulate the bioavailability, biodistribution, and pharmacokinetic characteristics of payload therapeutics [36–38]. Coating onto nanoparticles also prolongs half-life of the peptide in the circulation because clearance of the peptide by renal filtration is prevented, resulting in a longer period of activity at the target [39]. Thus, a multivalent, long-circulating form of iRGD could optimally combine both the selective drug delivery-enhancing and anti-metastatic activities of this peptide.

Overall, the results presented here demonstrate for the first time that a single dose of iRGD-NW when applied in the early stages of metastasis development can have a significant effect on metastatic tumor progression. Our results observed in two independent models of triple-negative breast cancer brain metastasis suggest that this targeted therapeutic has a promising role in the inhibition and prevention of brain metastases. As the molecular targets of the iRGD peptide are universally expressed in both preclinical models and human disease, we anticipate that this therapeutic should be easily translatable to the clinic.

Acknowledgments

This work was supported by the following: Cancer Center Support grant CA30199, and the Center for Cancer Nanotechnology Excellence and Translation U54 CA119367.

References

1. Lin NU. Breast cancer brain metastases: new directions in systemic therapy. Ecancermedicalscience. 2013; 7:307. [PubMed: 23662165]
2. Niikura N, Hayaski N, Masuda N, Takashima S, Nakamura R, Watanabe K, Kanbayashi C, Ishida M, Hozumi Y, Tsuneizumi M, et al. Treatment outcomes and prognostic factors for patients with brain metastases from breast cancer of each subtype: a multi-center retrospective analysis. Breast Cancer Res Treat. 2014; 147:103–112. [PubMed: 25106661]
3. Arvold ND, Oh KS, Niemierko A, Taghian AG, Lin NU, Abi-Raad RF, Sreedhara M, Harris JR, Alexander BM. Brain metastases after breast-conserving therapy and systemic therapy: incidence and characteristics by biologic subtype. Breast Cancer Res Treat. 2012; 136:153–160. [PubMed: 22968656]
4. Brooks PC, Clark RA, Cheresh DA. Requirement of vascular integrin alpha v beta 3 for angiogenesis. Science (New York, N Y). 1994; 264:569–571.
5. Lorger M, Krueger JS, O'Neal M, Staflin K, Felding-Habermann B. Activation of tumor cell integrin alphavbeta3 controls angiogenesis and metastatic growth in the brain. Proc Natl Acad Sci U S A. 2009; 106:10666–10671. [PubMed: 19541645]
6. Ruoslahti E. Specialization of tumour vasculature. Nat Rev Cancer. 2002; 2:83–90. [PubMed: 12635171]
7. Sugahara KN, Teesalu T, Karmali PP, Kotamraju VR, Agemy L, Girard OM, Hanahan D, Mattrey RF, Ruoslahti E. Tissue-penetrating delivery of compounds and nanoparticles into tumors. Cancer Cell. 2009; 16:510–520. [PubMed: 19962669]
8. Ruoslahti E, Pierschbacher MD. Arg-Gly-Asp: a versatile cell recognition signal. Cell. 1986; 44:517–518. [PubMed: 2418980]
9. Sugahara KN, Teesalu T, Karmali PP, Kotamraju VR, Agemy L, Greenwald DR, Ruoslahti E. Coadministration of a tumor-penetrating peptide enhances the efficacy of cancer drugs. Science. 2010; 328:1031–1035. [PubMed: 20378772]
10. Teesalu T, Sugahara KN, Ruoslahti E. Tumor-penetrating peptides. Front Oncol. 2013; 3:216. [PubMed: 23986882]
11. Agemy L, Friedmann-Morvinski D, Kotamraju VR, Roth L, Sugahara KN, Girard OM, Mattrey RF, Verma IM, Ruoslahti E. Targeted nanoparticle enhanced proapoptotic peptide as potential therapy for glioblastoma. Proc Natl Acad Sci U S A. 2011; 108:17450–17455. [PubMed: 21969599]
12. Yu KF, Zhang WQ, Luo LM, Song P, Li D, Du R, Ren W, Huang D, Lu WL, Zhang X, et al. The antitumor activity of a doxorubicin loaded, iRGD-modified sterically-stabilized liposome on B16-F10 melanoma cells: in vitro and in vivo evaluation. Int J Nanomedicine. 2013; 8:2473–2485. [PubMed: 23885174]
13. Sugahara K, Braun GB, de Mendoza TH, Kotamraju VR, French RP, Lowy AM, Teesalu T, Ruoslahti E. A tumor-specific tissue-penetrating peptide inhibits metastasis. AACR Anual Meeting LB-102. 2014
14. Murrell D, Foster PJ, Chambers AF. Brain metastases from breast cancer: lessons from experimental magnetic resonance imaging studies and clinical implications. J Mol Med (Berl). 2014; 92:5–12. [PubMed: 24306136]
15. Heyn C, Ronald JA, Ramadan SS, Snir JA, Barry AM, MacKenzie LT, Mikulis DJ, Palmieri D, Bronder JL, Steeg PS, et al. In vivo MRI of cancer cell fate at the single-cell level in a mouse model of breast cancer metastasis to the brain. Magn Reson Med. 2006; 56:1001–1010. [PubMed: 17029229]
16. Agemy L, Sugahara KN, Kotamraju VR, Gujraty K, Girard OM, Kono Y, Mattrey RF, Park JH, Sailor MJ, Jimenez AI, et al. Nanoparticle-induced vascular blockade in human prostate cancer. Blood. 2010; 116:2847–2856. [PubMed: 20587786]
17. Percy DB, Ribot EJ, Chen Y, McFadden C, Simedrea C, Steeg PS, Chambers AF, Foster PJ. In vivo characterization of changing blood-tumor barrier permeability in a mouse model of breast cancer metastasis: a complementary magnetic resonance imaging approach. Invest Radiol. 2011; 46:718–725. [PubMed: 21788908]

18. Heyn C, Ronald JA, Mackenzie LT, MacDonald IC, Chambers AF, Rutt BK, Foster PJ. In vivo magnetic resonance imaging of single cells in mouse brain with optical validation. Magn Reson Med. 2006; 55:23–29. [PubMed: 16342157]
19. Park JH, von Maltzahn G, Zhang L, Schwartz MP, Ruoslahti E, Bhatia SN, Sailor MJ. Magnetic iron oxide nanoworms for tumor targeting and imaging. Adv Mater. 2008; 20:1630–1635. [PubMed: 21687830]
20. Lockman PR, Mittapalli RK, Taskar KS, Rudraraju V, Gril B, Bohn KA, Adkins CE, Roberts A, Thorsheim HR, Gaasch JA, Huang S, Palmieri D, Steeg PS, Smith QR. Heterogeneous blood-tumor barrier permeability determines drug efficacy in experimental brain metastases of breast cancer. Clin Cancer Res. 2010; 16(23):5664–5678. [PubMed: 20829328]
21. Ribot EJ, Martinez-Santiesteban FM, Simedrea C, Steeg PS, Chambers AF, Rutt BK, Foster PJ. In vivo single scan detection of both iron-labeled cells and breast cancer metastases in the mouse brain using balanced steady-state free precession imaging at 1.5 T. J Magn Reson Imaging. 2011; 34:231–238. [PubMed: 21698713]
22. Perera M, Ribot EJ, Percy DB, McFadden C, Simedrea C, Palmieri D, Chambers AF, Foster PJ. In vivo magnetic resonance imaging for investigating the development and distribution of experimental brain metastases due to breast cancer. Transl Oncol. 2012; 5:217–225. [PubMed: 22741041]
23. Naumov GN, MacDonald IC, Weinmeister PM, Kerkvliet N, Nadkarni KV, Wilson SM, Morris VL, Groom AC, Chambers AF. Persistence of solitary mammary carcinoma cells in a secondary site: a possible contributor to dormancy. Cancer Res. 2002; 62:2162–2168. [PubMed: 11929839]
24. Fitzgerald DP, Emerson DL, Qian Y, Anwar T, Liewehr DJ, Steinberg SM, Silberman S, Palmieri D, Steeg PS. TPI-287, a new taxane family member, reduces the brain metastatic colonization of breast cancer cells. Mol Cancer Ther. 2012; 11:1959–1967. [PubMed: 22622283]
25. Vellon L, Menendez JA, Liu H, Lupu R. Up-regulation of alphavbeta3 integrin expression is a novel molecular response to chemotherapy-induced cell damage in a heregulin-dependent manner. Differentiation. 2007; 75:819–830. [PubMed: 17999741]
26. Levkau B, Kenagy RD, Karsan A, Weitkamp B, Clowes AW, Ross R, Raines EW. Activation of metalloproteinases and their association with integrins: an auxiliary apoptotic pathway in human endothelial cells. Cell Death Differ. 2002; 9:1360–1367. [PubMed: 12478473]
27. Stupack DG, Puente XS, Boutsaboualoy S, Storgard CM, Cheresh DA. Apoptosis of adherent cells by recruitment of caspase-8 to unligated integrins. J Cell Biol. 2001; 155:459–470. [PubMed: 11684710]
28. Kurozumi K, Ichikawa T, Onishi M, Fujii K, Date I. Cilengitide treatment for malignant glioma: current status and future direction. Neurol Med Chir (Tokyo). 2012; 52:539–547. [PubMed: 22976135]
29. Ruegg C, Dormond O, Mariotti A. Endothelial cell integrins and COX-2: mediators and therapeutic targets of tumor angiogenesis. Biochim Biophys Acta. 2004; 1654:51–67. [PubMed: 14984767]
30. Grandclement C, Borg C. Neuropilins: a new target for cancer therapy. Cancers (Basel). 2011; 3:1899–1928. [PubMed: 24212788]
31. Starzec A, Vassy R, Martin A, Lecouvey M, Di Benedetto M, Crepin M, Perret GY. Antiangiogenic and antitumor activities of peptide inhibiting the vascular endothelial growth factor binding to neuropilin-1. Life Sci. 2006; 79:2370–2381. [PubMed: 16959272]
32. Castro-Rivera E, Ran S, Brekken RA, Minna JD. Semaphorin 3B inhibits the phosphatidylinositol 3-kinase/Akt pathway through neuropilin-1 in lung and breast cancer cells. Cancer Res. 2008; 68:8295–8303. [PubMed: 18922901]
33. Nasarre C, Roth M, Jacob L, Roth L, Koncina E, Thien A, Labourdette G, Poulet P, Hubert P, Cremel G, et al. Peptide-based interference of the transmembrane domain of neuropilin-1 inhibits glioma growth in vivo. Oncogene. 2010; 29:2381–2392. [PubMed: 20140015]
34. Zhang L, Parry GC, Levin EG. Inhibition of tumor cell migration by LD22-4, an N-terminal fragment of 24-kDa FGF2, is mediated by Neuropilin 1. Cancer Res. 2013; 73:3316–3325. [PubMed: 23667176]

35. Pilch J, Habermann R, Felding-Habermann B. Unique ability of integrin alpha(v)beta 3 to support tumor cell arrest under dynamic flow conditions. J Biol Chem. 2002; 277:21930–21938. [PubMed: 11934894]

36. Saha RN, Vasanthakumar S, Bende G, Snehalatha M. Nanoparticulate drug delivery systems for cancer chemotherapy. Mol Membr Biol. 2010; 27:215–231. [PubMed: 20939772]

37. Peng XH, Qian X, Mao H, Wang AY, Chen ZG, Nie S, Shin DM. Targeted magnetic iron oxide nanoparticles for tumor imaging and therapy. Int J Nanomedicine. 2008; 3:311–321. [PubMed: 18990940]

38. Min KH, Lee HJ, Kim K, Kwon IC, Jeong SY, Lee SC. The tumor accumulation and therapeutic efficacy of doxorubicin carried in calcium phosphate-reinforced polymer nanoparticles. Biomaterials. 2012; 33:5788–5797. [PubMed: 22591612]

39. Ruoslahti E. Peptides as targeting elements and tissue penetration devices for nanoparticles. Adv Mater. 2012; 24:3747–3756. [PubMed: 22550056]

Key messages

- bSSFP MRI can be used to track nonproliferative iron-labeled cells and tumor development over time.
- iRGD-NW, when applied early, has a significant effect on metastatic tumor progression.
- Retained signal voids represent a subpopulation of nonproliferating tumor cells.
- Reduced cell retention and tumor burden show a role for iRGD-NW in metastasis prevention.
- iRGD target is universally expressed; thus, iRGD-NW should be clinically translatable.

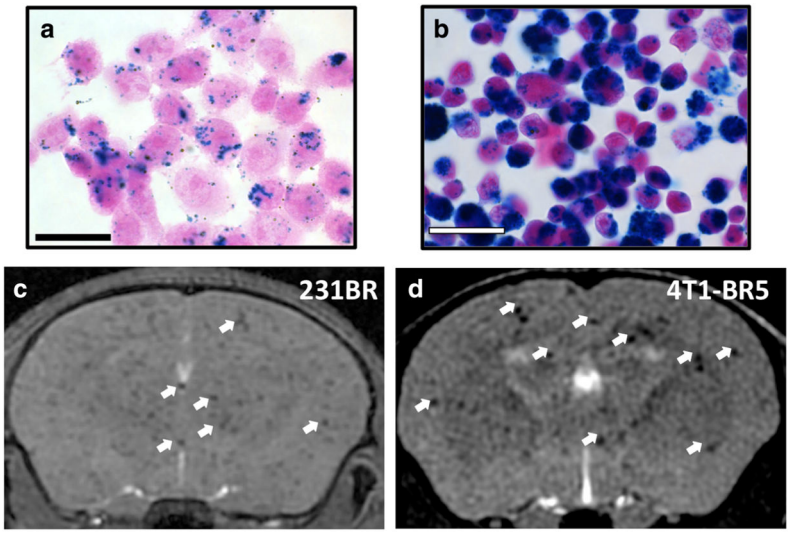

Fig. 1.

Visualization of the delivery of IO-labeled cells to mouse brain by bSSFP MRI. 231BR (**a**) and 4T1-BR5 (**b**) cells stained with PPB and counterstained with NFR to detect the presence of iron labeling. Intracellular iron (*blue*) was detected in the cytoplasm of IO-labeled cells. Representative images are shown. Magnification, ×40; *scale bar*=30 μm. **c** Axial MR image of a mouse within 24 h after injection with 1.5×10^5 IO-labeled 231BR cells. **d** Axial MR image of mouse within 24 h after injection with 2×10^4 IO-labeled 4T1-BR5 cells. *White arrows* indicate examples of signal void

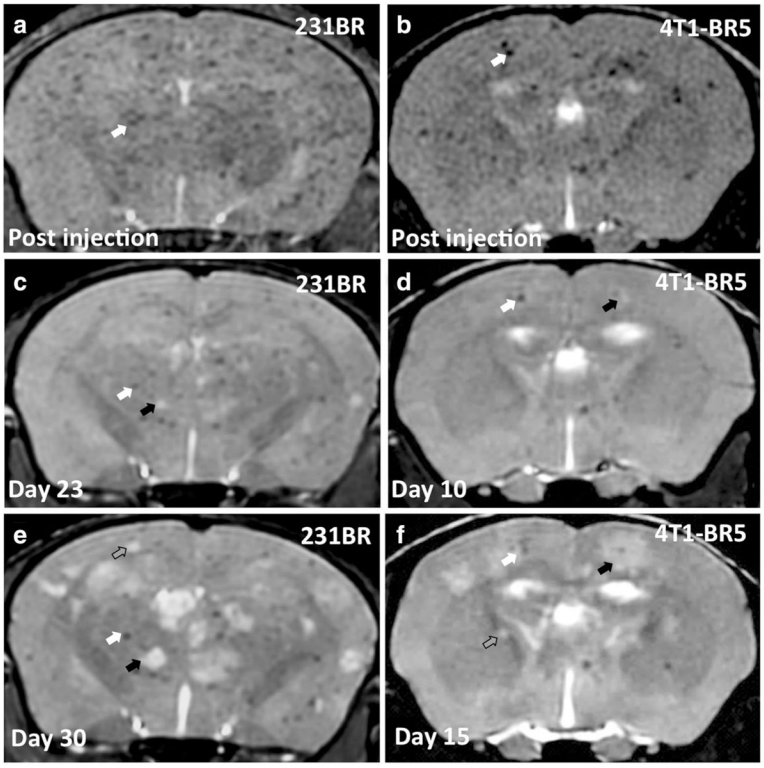

Fig. 2.

bSSFP MRI can be used to visualize the development of brain metastases and retention of signal voids over time. Axial MR image of a representative mouse brain within 24 h (**a**), 23 days (**c**), and 30 days (**e**) after injection with 1.5×10^5 IO-labeled 231BR cells. The example mouse was injected intravenously with saline at day 12. Axial MR image of a representative mouse brain within 24 h (**b**), 10 days (**d**), and 15 days (**f**) after injection with 2×10^4 IO-labeled 4T1-BR5 cells. *White arrows* indicate examples of voids that are retained over time. *Black arrows* indicate examples of metastases that increase in volume over time. *Gray arrows* indicate examples of metastases first seen at the late MR time point

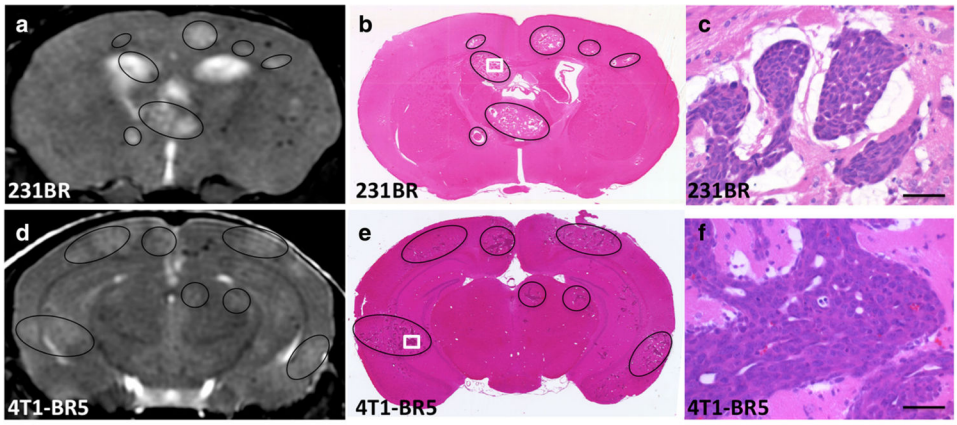

Fig. 3.

Tumors identified by bSSFP MR imaging correlate well with those seen in H&E-stained tissue sections. Representative MR images (**a**) and H&E-stained brain sections (**b**) of 231BR tumor-bearing nude mice brain at endpoint. Representative MR images (**d**) and H&E-stained brain sections (**e**) of a 4T1-BR5 tumor-bearing BalbC mice brain at endpoint. *Black circles* delineate tumors. *White boxes* indicate site of high-magnification images seen in **c** and **f**. Areas of edema were evident as large white spaces in H&E-stained sections. *Scale bar*=50 μm

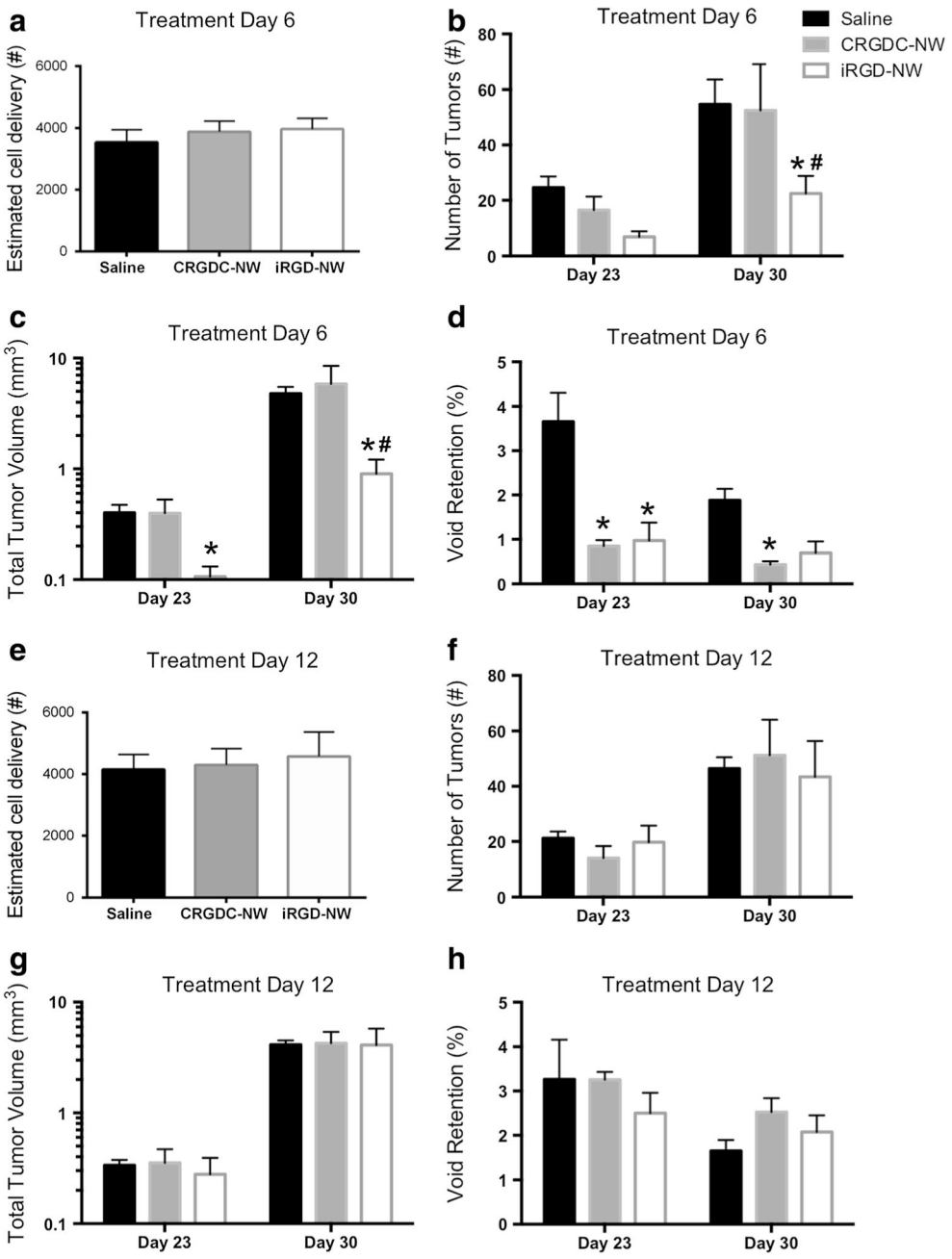

Fig. 4.

Quantification of cell delivery, tumor number, total tumor volume, and signal void retention in saline, CRGDC-, and iRGD-NW-injected nu/ nu mouse brain from MR images acquired on day 23 and day 30 post-231BR cell injection. **a** Signal voids were quantified to estimate the cell delivery achieved for each experimental mouse injected with 1.5×10^5 IO-labeled 231BR cells. There was no statistically significant difference in cell delivery in the mouse groups. **b** Number of tumors observed in mice treated with saline CRGDC-NW or iRGD-NW at 6 days post-cell injection. Two-way ANOVA; time $p=0.0747$, treatment $p<0.0001$. **c** Total tumor volume seen in mice treated at 6 days post-cell injection. Two-way ANOVA;

time p=0.0011, treatment p=0.0491. **d** Retention of signal voids in mice treated at 6 days post-cell injection. Two-way ANOVA; time p=0.0013, treatment p=0.0002. **e** Signal voids were quantified to estimate the cell delivery achieved for each experimental mouse injected with 1.5×10^5 IO-labeled 231BR cells. There was no statistically significant difference in cell delivery in the mouse groups examined. Mice were injected with saline, CRGDC-NW, or iRGD-NW at day 12. **f** Number of tumors observed in mice treated with saline, CRGDC-NW, or iRGD-NW at 12 days post-cell injection. Two-way ANOVA; time p=0.0004, treatment p=0.9715. **g** Total tumor volume seen in mice treated at 12 days post-cell injection. Two-way ANOVA; time p<0.0001, treatment p= 0.9908. **h** Retention of signal voids in mice treated at 12 days post-cell injection. Two-way ANOVA; time p=0.0038, treatment p=0.5889. **a**–**d** n=6 per group, **e**–**h** n=5 per group. *Significantly different than respective saline control, #significantly different than respective CRGDC-NW

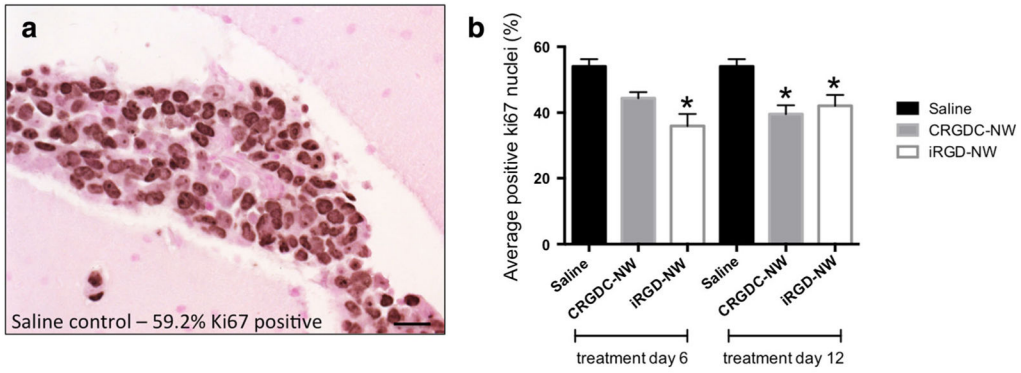

Fig. 5.

Tumors of mice treated with vehicle, CRGDC-NWs, and iRGD-NWs show differential expression of the proliferation marker Ki67. **a** An example image of Ki67 IHC staining in a saline-treated 231BR tumor with 59.2 % positive staining (*dark*) nuclei. *Scale bar*=20 μm. **b** Average Ki67-positive nuclear staining in endpoint tumors from mice treated at days 6 and 12. *Statistically different from saline control, one-way ANOVA $p<0.0001$

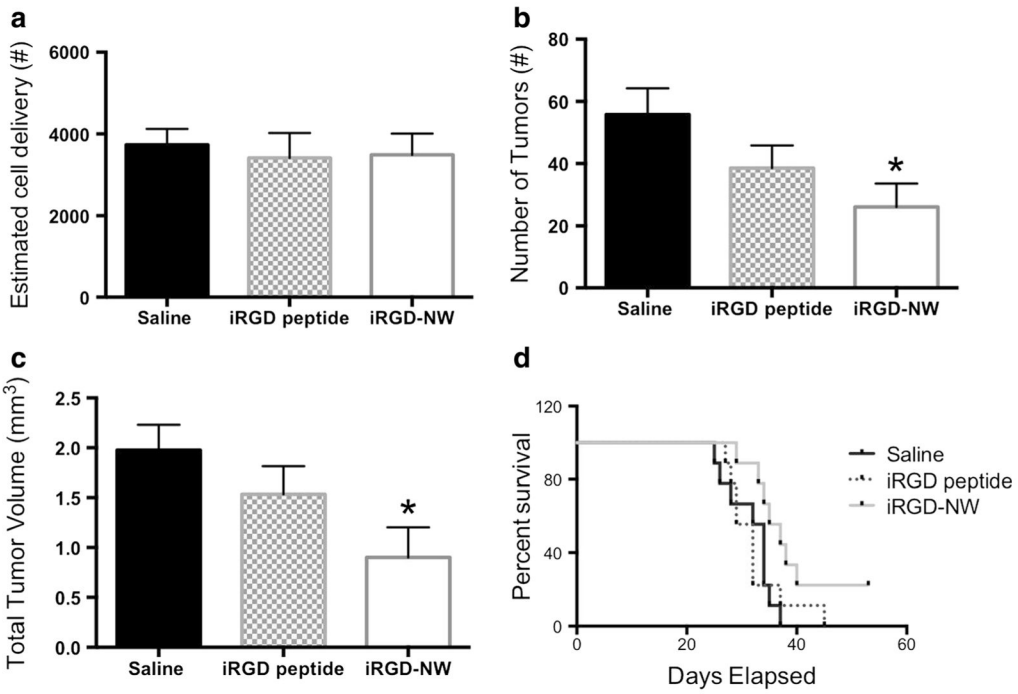

Fig. 6.

Comparison of cell delivery, tumor number, total tumor volume, and overall survival in mice treated with saline, free iRGD peptide, or iRGD-NWs (*n*=9 per group). **a** Signal voids were quantified to estimate the cell delivery achieved for each experimental mouse injected with 1.5×10^5 IO-labeled 231BR cells. There was no statistically significant difference in cell delivery in the mouse groups. **b** Number of tumors observed in mice imaged at 25 days post-cell injection. One-way ANOVA; time p=0.0389. **c** Total tumor volume observed in mice imaged at 25 days post-cell injection. One-way ANOVA; time p=0.0351. **d** Kaplan-Meier survival analysis of mice treated with saline, free iRGD peptide, or iRGD-NWs. Mantel-Cox test ns p=0.1085, logrank test for trend p=0.043

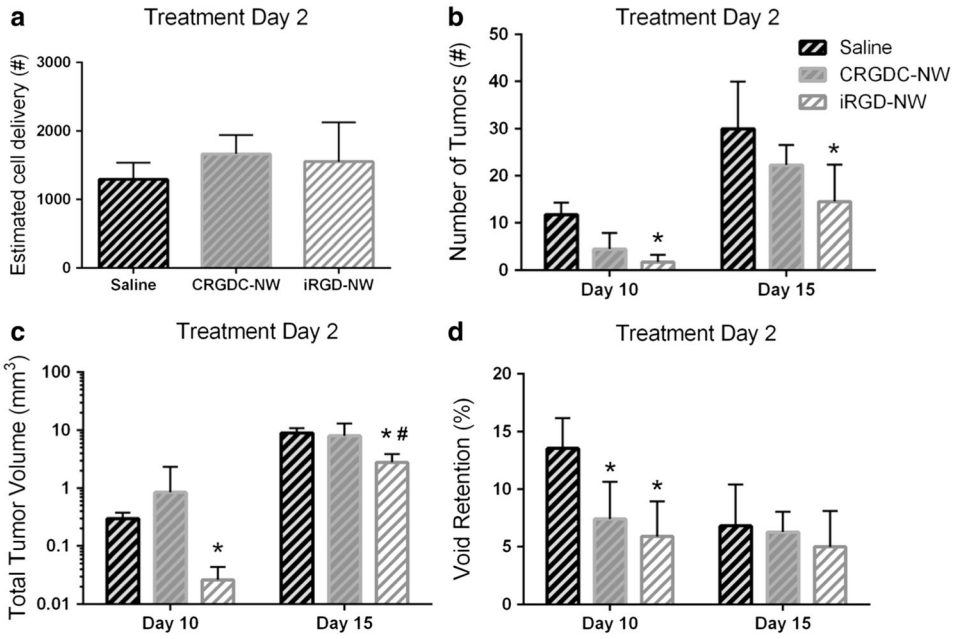

Fig. 7.

Quantification of cell delivery, tumor number, total tumor volume, and signal void retention in the brains of mice injected with saline, CRGD C-NW, or iRGD-NW. MR images acquired on day 10 and day 15 post-4T1-BR5 cell injection are shown. **a** Signal voids were quantified to estimate the cell delivery achieved for each experimental mouse injected with 2×10^4 IO-labeled 4T1-BR5 cells. There was no statistically significant difference in cell delivery among the experimental groups. **b** Number of tumors observed in mice treated at 2 days post-cell injection. Two-way ANOVA; time $p<0.0001$, treatment $p=0.0051$. **c** Total tumor volume in mice treated at 2 days post-cell injection; two-way ANOVA; time $p<0.0001$, treatment $p=0.0209$. **d** Retention of signal voids in mice treated at 6 days post-cell injection. Two-way ANOVA; time $p<0.0001$, treatment $p=0.0005$